Electronic Supplementary Material

Angle-tunable intersubband photoabsorption and enhanced photobleaching in twisted bilayer graphene

Eva A. A. Pogna[1], Xianchong Miao[2], Driele von Dreifus[3], Thonimar V. Alencar[4], Marcus V. O. Moutinho[5], Pedro Venezuela[6], Cristian Manzoni[7], Minbiao Ji[2] (✉), Giulio Cerullo[7] (✉), and Ana Maria de Paula[3] (✉)

[1] *Istituto di Nanoscienze CNR-NANO, Laboratory NEST, Piazza San Silvestro 12, Pisa 56127, Italy*
[2] *State Key Laboratory of Surface Physics and Department of Physics, Fudan University, Shanghai 200433, China*
[3] *Departamento de Física, Instituto de Ciências Exatas, Universidade Federal de Minas Gerais, Belo Horizonte-MG 31270-901, Brazil*
[4] *Departamento de Física, Instituto de Ciências Exatas e Biológicas, Universidade Federal de Ouro Preto, Ouro Preto-MG 35400-000, Brazil*
[5] *Núcleo Multidisciplinar de Pesquisas em Computação - NUMPEX-COMP, Campus Duque de Caxias, Universidade Federal do Rio de Janeiro, Duque de Caxias-RJ 25265-970, Brazil*
[6] *Instituto de Física, Universidade Federal Fluminense, UFF, Niterói-RJ 24210-346, Brazil*
[7] *IFN-CNR, Dipartimento di Fisica, Politecnico di Milano, Piazza L. da Vinci 32, Milano 20133, Italy*

Supporting information to https://doi.org/10.1007/s12274-021-3288-0

1 Twist angle estimation from E_{vHs}

The electronic band structure and the corresponding density of states are evaluated for different twist angles. The energy position of the calculated vHs and ISB electronic transitions for holes and electrons are reported in Fig. S1 as function of the twist angle.

In analogy with Ref. 1 we find a convenient expression of θ fitting the theoretical data in the inset in the range $6.8° < \theta < 8.6°$ with the function $\theta\,[°] = A\text{-}\sqrt{(B\text{-}C\,E_{vHs}\,[eV])}$, with $A = 45.380$, $B = 2.030 \times 10^3$, $C = 4.186 \times 10^2$.

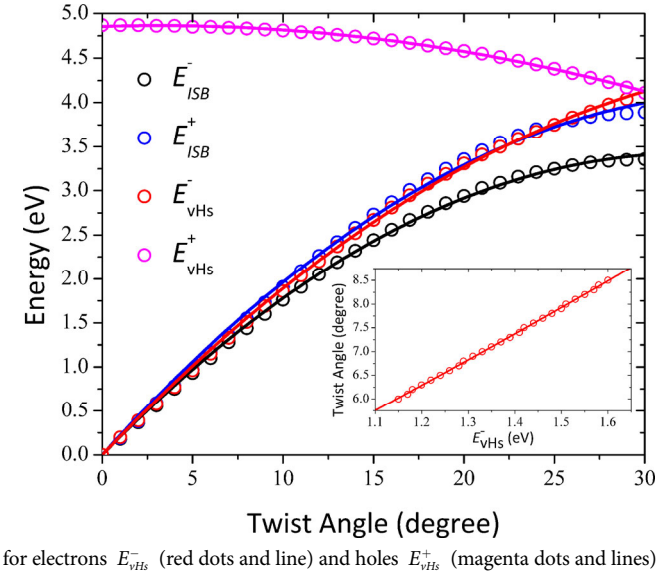

Figure S1 Calculated energy of vHs for electrons E^-_{vHs} (red dots and line) and holes E^+_{vHs} (magenta dots and lines) and of ISB transitions for electrons E^-_{ISB} (black dots and lines) and holes E^+_{ISB} (blue dots and lines) as a function of the twist angle. The inset shows for the vHs energy in our experimental region of twist angles together with the best fit function (red solid line).

To calculate the uncertainty in the angle estimation we derive the expression:

$$\delta\theta[°] = \frac{C}{2\sqrt{B - C\,E_{vHs}\,[eV]}}\delta E$$

considering the δE as the uncertainty in the PLE peak position. From the PLE results, the fitted Gaussians give $\delta E \leq 0.01$ eV for all the stacks. For the bilayer stack with $E_{vHs} = 1.388 \pm 0.007$ eV, for example, we find that $\theta = 7.31° \pm 0.04°$.

Address correspondence to Minbiao Ji, minbiaoj@fudan.edu.cn; Giulio Cerullo, giulio.cerullo@polimi.it; Ana Maria de Paula, ana@fisica.ufmg.br

2 Fluence dependence of transient absorption spectra

The ISB transitions energetically overlap with the IB optical transitions. The hot-electron distribution causes simultaneously the bleaching of IB absorption due to Pauli blocking and the activation of ISB absorption with contributions to the transient transmissivity of opposite signs. The interplay of these contributions depends on the fluence and, at high density of photo-excited carriers, we observe that the bleaching is dominating over the photo-induced absorption over the entire probe photon energy range.

Accordingly, while the TA of SLG scales linearly with fluence, the spectra of tBLG change shape with fluence, as reported in Fig. S2(a) for four different tBLG samples. The dynamics as function of pump-probe delay and probe wavelength is reported in Fig. S2(b) at the two compared fluences for the stack with $\theta = 7.93°$, taken as prototype of tBLG.

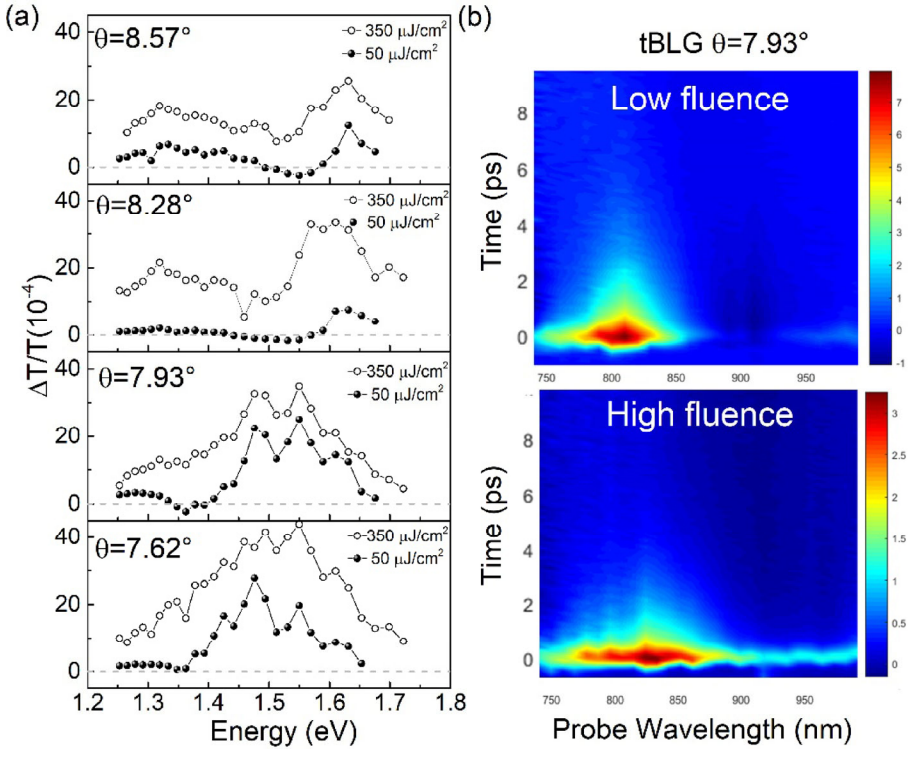

Figure S2 (a) $\Delta T/T$ spectra of tBLG at incident fluence of 350 μJ cm^{-2} (open symbols) and 50 μJ cm^{-2} (full symbols) for different twist angles θ; (b) $\Delta T/T$ as a function of probe wavelength and time delay at low incident fluence 50 μJ cm^{-2} (upper panel) and high incident fluence 350 μJ cm^{-2} (lower panel) for the tBLG with $\theta = 7.93°$.

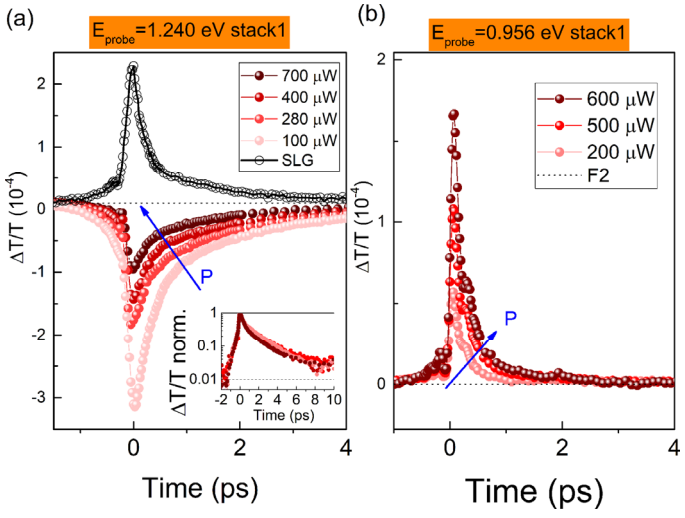

Figure S3 Transient transmissivity dynamics at different excitation power at probe photon energy (a) E_{probe} = 1.240 eV corresponding to the ISB and (b) E_{probe} = 0.958 eV in the low-energy PB band. Normalised dynamics at E_{probe} = 1.240 eV are reported in the inset of panel a.

While the photobleaching signal increases with excitation power, due to the increase in initial electron temperature and to the superlinear dependence of $\Delta T/T$ on T_e, the instantaneous PA signal decreases. In Fig. S3 we report the pump power dependence of relaxation dynamics of the stack with $\theta = 7.31°$ at probe energy E_{probe} = 1.240 eV corresponding to the ISB, and E_{probe}= 0.956 eV in the low-energy PB band.

3 Calculation of the electron temperature

In order to obtain the electron and phonon temperatures as a function of time we adopt a three temperature model [2]. This model considers that after a transition to an out-of-equilibrium state the electrons rapidly exchange energy with phonons via electron-phonon interaction achieving a quasi-equilibrium Fermi distribution. Considering the occupation number of electrons and phonons as Fermi-Dirac and Bose-Einstein distributions respectively, we can associate an effective temperature for the electrons, T_e, and for phonons, T_v which are separated into strongly coupled (v = sc) and weakly coupled (v = wc) phonons. Thus, a system of coupled equations for the three temperatures (T_e, T_{sc}, T_{wc}) is used to simulate the dynamics of the electrons and phonons after the laser pulse excitation. For a Gaussian pulse $I(t)$ with fluence F and pulse duration τ_p, the temporal dependence of the effective temperatures is given by:

$$\begin{aligned}
\frac{dT_e}{dt} &= \frac{I(t)}{\beta c_e} - \frac{g_{sc}}{c_e}(T_e - T_{sc}) - \frac{g_{wc}}{c_e}(T_e - T_{wc}) \\
\frac{dT_{sc}}{dt} &= \frac{g_{sc}}{c_{sc}}(T_e - T_{sc}) - \frac{1}{\tau_o}(T_{sc} - T_{wc}) \\
\frac{dT_{wc}}{dt} &= \frac{g_{wc}}{c_{wc}}(T_e - T_{wc}) + \frac{c_{sc}}{c_{wc}\tau_o}(T_{sc} - T_{wc})
\end{aligned} \tag{1}$$

where β is a dimensionless parameter which determines the fraction of the pulse energy absorbed by the electrons and τ_o = 2.5 ps is the optical phonon lifetime [3-4]. The respective specific heats for the electrons (c_e), strongly coupled phonons (c_{sc}) and weakly coupled phonons (c_{wc}) are obtained by the following integrals:

$$c_e = \int_{-\infty}^{\infty} \epsilon N(\epsilon) \frac{\partial f_D(\epsilon, T_e)}{\partial T_e} d\epsilon \tag{2}$$

$$c_v = \int_{0}^{\infty} \omega F_v(\omega) \frac{\partial n_B(\omega, T_v)}{\partial T_v} d\omega \tag{3}$$

Here, $N(\epsilon)$ and $F_v(\omega)$ are the density of states for electrons, strongly coupled (v = sc) and weakly coupled (v = wc) phonons obtained, for both SLG and tBLG, from tight-binding [5,6] and force constant [7] methods parameterized by first principles calculations, and f_D (n_B) is the Fermi-Dirac (Bose-Einstein) distribution. The difference between weakly and strongly coupled phonons in graphene is addressed considering that the optical A'$_1$ (TO) and E$_{2g}$ (LO) phonons in the vicinity of K and Γ points of the Brillouin zone are those with high electron-phonon coupling. In this way, in our model for SLG, only phonons with frequency close to (1350 ± 2) cm^{-1} and (1580 ± 2) cm^{-1} are considered in the calculation of the strongly coupled quantities, while the other modes are used for the weakly coupled ones. For tBLG, the additional low frequency and high density phonon modes close to ZA$_2$ (88 ± 2) cm^{-1} at the Γ point are also considered as strongly coupled phonons. This mode is not present in the SLG because its polarization represents the out-of-plane breathing between two adjacent layers due to the weak van der Waals interaction.

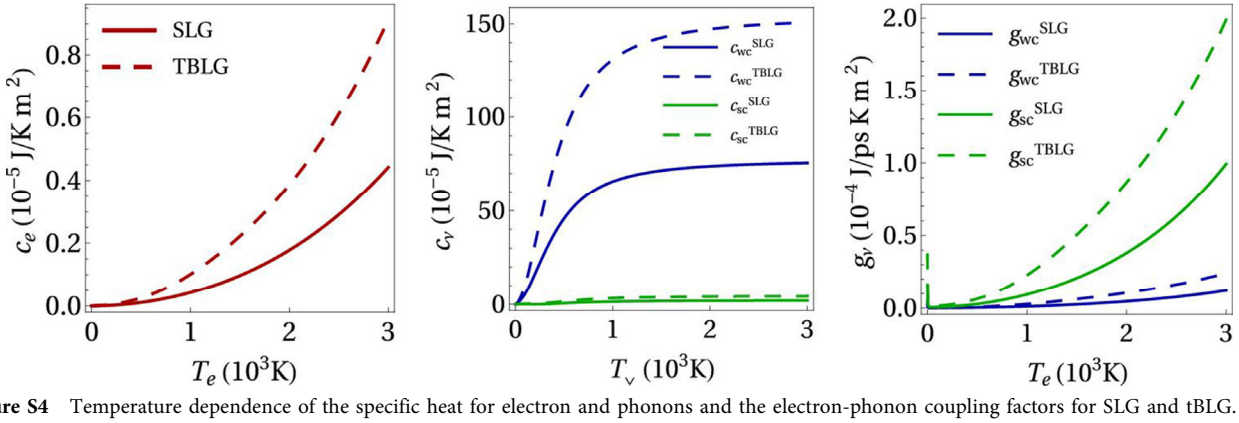

Figure S4 Temperature dependence of the specific heat for electron and phonons and the electron-phonon coupling factors for SLG and tBLG. The indexes *sc* and *wc* stand for strongly coupled and weakly coupled phonons, respectively.

The temperature dependent electron-phonon coupling factor can be calculated as in Ref. 8 by:

$$g_v = -\frac{\pi\hbar k_B \lambda_v \langle\omega^2\rangle_v}{N(\epsilon_F)} \int_{-\infty}^{\infty} N^2(\epsilon) \frac{\partial f_D(\epsilon, T_e)}{\partial \epsilon} d\epsilon \tag{4}$$

Figure S4 shows the temperature dependence of the specific heat for electron and phonons and the electron-phonon coupling factors for SLG and tBLG. We used $\lambda_{sc}\langle\omega^2\rangle_{sc}$ = 566 meV^2 and $\lambda_{wc}\langle\omega^2\rangle_{wc}$ = 69 meV^2, that are the same used for SLG [2].

Figure S5 shows the evolution of the effective temperatures for an incident fluence of 50 μJ cm^{-2} and a pulse duration τ_p = 200 fs. To consider the difference in optical absorption for SLG and tBLG, we used β = 50 for the former and β = 25 for the latter. These values were chosen to compare with the experimental results.

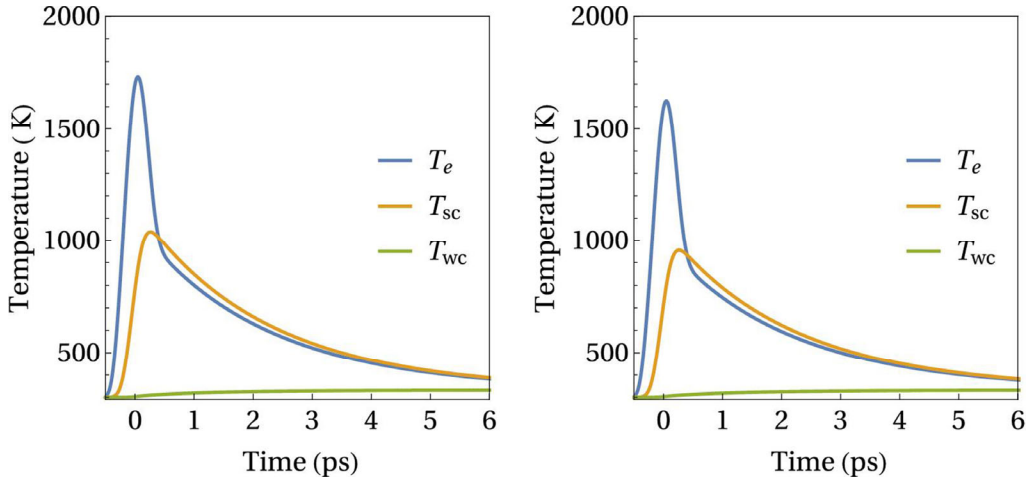

Figure S5 The temporal evolution of the electron and phonon effective temperatures after excitation for a laser fluence of 50 μJ cm^{-2}.

4 Relaxation dynamics of tBLG stacks

Similar relaxation dynamics is measured in all the probed tBLG stacks presented in Figures 2 and 3 as long as the probe energy is tuned to match the energy of the three different bands we have discussed. The dynamics of tBLG are reported in Fig. S6 as colored dots compared to that of SLG, displayed as black symbols. The probe energies are specified in the graphs, and correspond to the vHs (pink dots), the peak of the PA band (red symbols) and the low energy tail (blue).

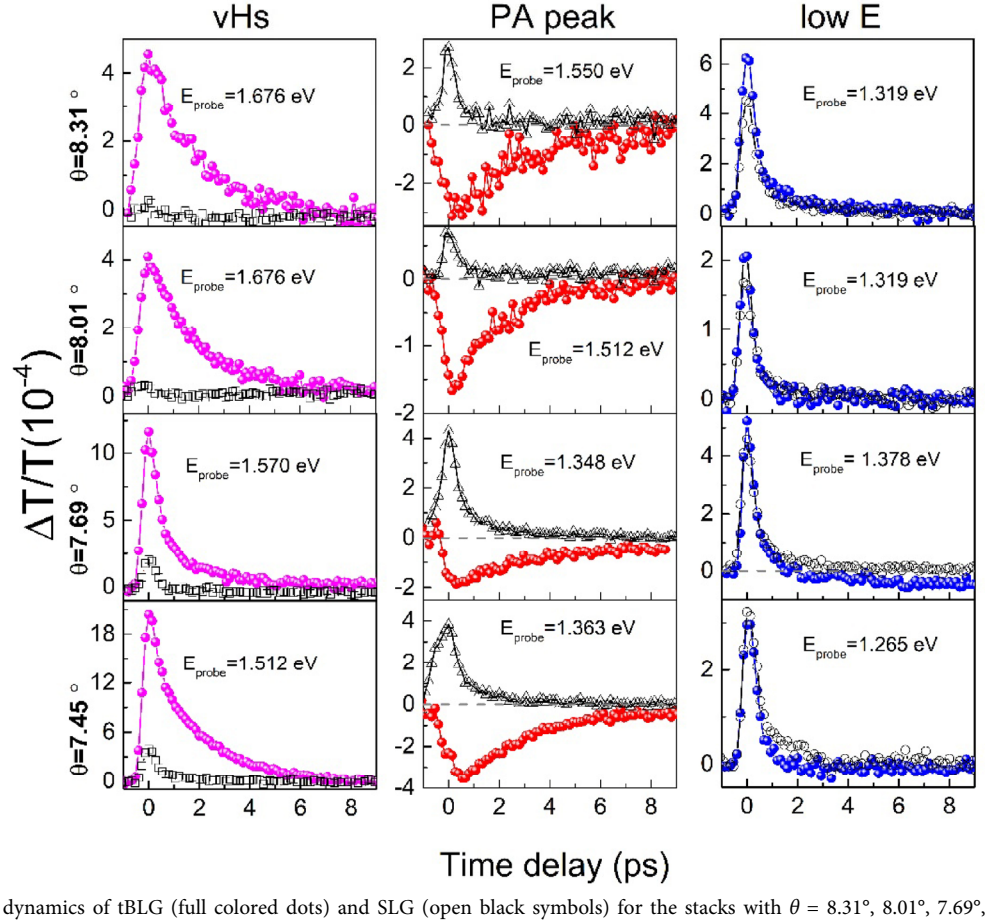

Figure S6 *ΔT/T* dynamics of tBLG (full colored dots) and SLG (open black symbols) for the stacks with θ = 8.31°, 8.01°, 7.69°, 7.45°, at the probe energies indicated in the graphs.

References

[1] Havener, R. W.; Liang, Y.; Brown, L.; Yang, L.; Park, J. Van Hove Singularities and Excitonic Effects in the Optical Conductivity of Twisted Bilayer Graphene. *Nano Lett.* **2014**, *14*, 3353-3357.

[2] F. Caruso, F.; Novko, D; Draxl, C. Photoemission signatures of nonequilibrium carrier dynamics from first principles. *Phys. Rev. B* **2020**, *101*, 035128.

[3] Wang, H. et al.Ultrafast relaxation dynamics of hot optical phonons in graphene. *App. Phys. Lett.* **2010**, *96*, 081917.

[4] Rana, F.; George, P. A.; Strait, J. H.; Dawlaty, J.; Shivaraman, S.; Chandrashekhar, M.; Spencer, M. G. et al. Carrier recombination and generation rates for intravalley and intervalley phonon scattering in graphene. *Phys. Rev. B* **2009**, *79*, 115447.
[5] Venezuela, P.; Lazzeri, M; Mauri, F. Theory of double-resonant Raman spectra in graphene: Intensity and line shape of defect-induced and two-phonon bands. *Phys. Rev.B* **2011**, *84*, 035433.
[6] Vela, A.; Moutinho, M.; Culchac, F.; Venezuela, P.; Capaz, R. B. Electronic Structure and Optical Properties of Twisted Multilayer Graphene. *Phys. Rev. B* **2018**, *98*, 155135.
[7] Cocemasov, A.I.; Nika, D.L.; Balandin,A. A. Phonons in twisted bilayer graphene. *Phys. Rev. B* **2013**, *88*, 035428.
[8] Wang, X. Y.; Riffe, D. M.; Lee, Y.-S.; Downer, M. C. Time-resolved electron-temperature measurement in a highly excited gold target using femtosecond thermionic emission. *Phys. Rev. B* **1994**, *50*, 8016-8019.